



Received 24 July 2024

Accepted 21 November 2024

Edited by F. Meilleur, Oak Ridge National Laboratory, USA, and North Carolina State University, USA

Keywords: space groups; asymmetric units; graph neural networks; powder X-ray diffraction; XRD; formation energies; property prediction.

Supporting information: this article has supporting information at journals.iucr.org/j

ASUGNN: an asymmetric-unit-based graph neural network for crystal property prediction

Barnie Cao,^{a*} Daniel Anderson^b and Luke Davis^b

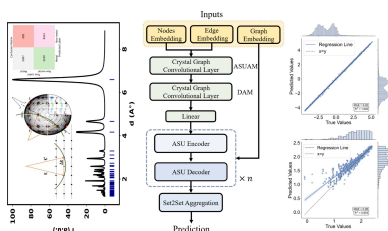
^aAdvanced Materials Thrust, Hong Kong University of Science and Technology, Guangzhou 511400, People's Republic of China, and ^bInternational Centre of Quantum and Molecular Structures, Shanghai University, Shanghai 200444, People's Republic of China. *Correspondence e-mail: barniecao@outlook.com

Material properties can often be derived directly from fundamental equations governing electron behavior. In this study, we present an open-source asymmetric-unit-based graph neural network designed to capture atomic patterns and their corresponding electron distributions. By coarse-graining sites belonging to conjugate subgroups and analyzing reciprocal space through powder X-ray diffraction patterns, our model predicts key physical properties, including formation energy, band gap, bulk modulus and metal/non-metal classification. Our method demonstrates exceptional predictive accuracy for properties calculated using density functional theory across the Materials Project dataset. Our approach is compared with state-of-the-art models and exhibits impressively low error rates in zero-shot predictions.

1. Introduction

Crystals exemplify a unique and precisely structured form of matter, composed of atoms or molecules arranged in a systematic pattern. This structured order is defined by the combination of known elements categorized into 230 space groups, meaning an almost limitless variety of crystal structures. This variability is further influenced by factors such as solid solution, degree of crystallinity, morphology and various other determinants. The spatial arrangement of the nuclei is determined by the lowest energy state of the electrons and, conversely, the spatial structure of the nuclei establishes the external potential that governs the Schrödinger equation for electrons, thus delineating the structural properties (Martin, 2020). In materials science, particularly when establishing a correspondence between a material's performance and its fundamental composition, the properties of a solid are intricately linked to its crystal structure. The successful prediction of crystal physical properties could significantly impact various fields, including the discovery of new materials, advancements in energy storage technologies and innovations in drug design. However, this task is exceptionally challenging, involving the understanding of the collective behavior of electrons (Bloch *et al.*, 2022).

Although material properties can be directly inferred from electron structure calculations such as density functional theory (DFT), relying solely on DFT calculations can prove highly resource intensive and time consuming. Consequently, numerous methods for predicting crystal properties have been developed (Xie & Grossman, 2018; Chen *et al.*, 2019; Kaba & Ravanbakhsh, 2022; Yan *et al.*, 2022; Choudhary & DeCost, 2021; Louis *et al.*, 2020). The integration of machine learning (ML) into property prediction has inaugurated a new interdisciplinary approach characterized by more efficient crystal



research papers

structure analysis, with computational speeds orders of magnitude faster than those achievable with DFT.

Xie & Grossman (2018) developed the crystal graph convolutional neural network (CGCNN) to learn material properties directly from atomic connections in crystals, marking an early use of graph neural networks (GNNs) in crystal studies. MEGNet (Chen *et al.*, 2019) links crystal structures to formation enthalpies with 86.2% accuracy. The atomistic line graph neural network (ALIGNN) (Choudhary & DeCost, 2021) uses both interatomic bonds and bond angles, improving predictions by efficiently incorporating angle information. Chen & Ong (2022) introduced M3GNet, a universal interatomic potential trained on extensive data, capable of identifying 1.8 million stable materials from 31 million hypothetical structures. Merchant *et al.* (2023) developed GNoME for large-scale active learning and structural prediction, achieving an 11 meV per atom error in formation energy and discovering over 2.2 million stable crystal structures with a stable prediction rate above 80%.

Structure representations enable novel crystal screening and generation. Many studies have used symmetry-enhancing methods to discover new crystals. Goodall *et al.* (2022) reduced the infinite atomic search space to a combinatorially enumerable one, using coordinate-free sets of symmetry-related positions as ML inputs. Their approach proved effective for identifying theoretically stable materials. Zhu *et al.* (2023) proposed a framework that combines Wyckoff position encoding with DFT to generate symmetry-compliant and stable inorganic crystals. This approach selectively generates materials by encoding the Wyckoff representation, thereby facilitating the discovery of novel materials and accurately predicting ground state and polymorphic structures. Similarly,

Jiao *et al.* (2024) applied space group constraints via lattice matrix and Wyckoff positions, achieving favorable crystal structure predictions with a novel denoising model.

The rapid advancements in crystal representation learning emphasize the growing focus on crystals' invariance to three-dimensional spatial symmetry operations, such as rotation, translation *etc*. Crystal representation for property prediction does not need to account for the generation of explicit expressions, allowing for a broader exploration of three-dimensional space embeddings. Three key elements require clarification in expressing crystals for ML purposes: (1) the spatial arrangement of distinct atoms and their interconnections in Cartesian coordinates; (2) the incorporation of symmetry constraints from crystal nature; and (3) the governing equation for electrons, namely, the Schrödinger equation. These aspects collectively determine the external potential, the quantization condition and the density of electron states in the ground state, thereby influencing the physical properties of ideal crystals.

In this study, we present ASUGNN, an open-source graph neural network designed to capture atomic patterns and their corresponding electron distributions. Our work positions the asymmetric unit (ASU) as the central element, inherently advantaged in symmetry preservation. By introducing strong constraints from Wyckoff sites, we apply a definitive indicator to crystal embedding through the proposed ASU adjacency matrix, masking the positional information belonging to the same conjugate subgroups. This approach enables the model to focus on learning the arrangement and distribution within the ASU, rather than grappling with complex, well established symmetry operations. Furthermore, we used ideal powder X-ray diffraction (XRD) patterns as the global embedding for

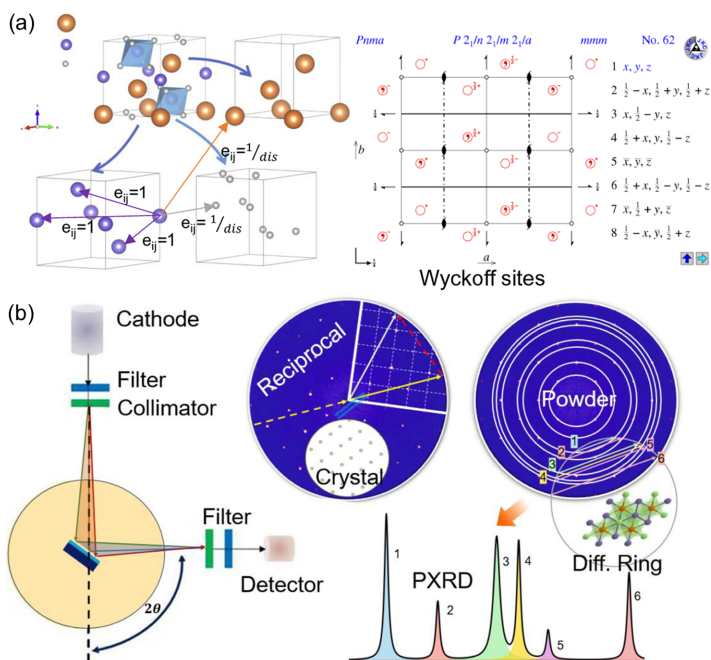


Figure 1

Physical embedding of ASUGNN for crystal property prediction. (a) ASU adjacency matrix, defined by coarse-graining, which does not differentiate atoms within the same conjugate subgroups. (b) The simulated ideal powder XRD generation process serves as a fingerprint, reflecting interactions between ions and electrons while incorporating reciprocal space insights. (c) Graph message-passing architecture in ASUGNN.

crystal graphs, ensuring a substantive capture of subtle variations in atomic pairs and making ASUGNN superior in understanding crystal clusters formed under phase transformations. Fig. 1 illustrates the graph embedding of ASUGNN for crystals. The atoms within a conventional unit cell (referred to as the lattice cell) of a crystal are retrieved as individual nodes and categorized by the Wyckoff sites into different ASUs, as shown in Fig. 1(a). Two adjacency matrices are defined: one for the real distances between each pair of atoms and one masked adjacency matrix which embodies strong connections for atoms that can be symmetrically equivalent under the space group. Furthermore, powder XRD reflects electron distributions across various atomic arrangements and incorporates insights from reciprocal space. The global insights of XRD and symmetry constraints from the ASU adjacency matrix are introduced in the graph message passing in ASUGNN, as shown in Fig. 1(c).

2. Graph embedding

To integrate these three key points, we employed an ASU-based framework within the GNN. Utilizing a message-passing mechanism, we iteratively update the network's understanding to encompass the governing equations of electrons, thereby facilitating accurate predictions.

2.1. Node (V)

In ASUGNN, each atom within a lattice cell is represented as an individual node with a 106-dimensional embedding. The first 92 dimensions replicate the CGCNN embedding (Xie & Grossman, 2018), reflecting the diverse physical properties of different elements. Additionally, ASUGNN node embedding incorporates features such as fractional atomic coordinates, lattice geometry (lattice constants), space group, ASU number, total atom count, lattice volume and average atomic mass. This results in a comprehensive 106-dimensional representation for each node. ASUGNN embeds both the specific attributes of each atom and their relative positions in Cartesian coordinates, along with the global spatial properties of the lattice in the node attributes. Detailed node attributes are provided in the supporting information.

2.2. Edge (E)

ASUGNN defines atomic connections using two adjacency matrices. The first is the distance adjacency matrix (DAM), an $N \times N$ matrix (where N is the number of nodes), which records the absolute distances between atom pairs in Cartesian coordinates. The second matrix, the ASU adjacency matrix (ASUAM), is a group-based weight matrix that enforces symmetry constraints from the space group. Atoms occupying equivalent sites within a conjugate subgroup are considered indistinguishable and are strongly connected, with an edge weight of 1 assigned between them. For atoms a_i and a_j , if they occupy equivalent sites, the edge weight is set to 1. Otherwise, the edge weight is determined by the inverse of their Cartesian distance.

Atom-to-atom distances typically exceed 1 Å, approximately the diameter of a hydrogen atom (Bohr, 1913), leading to edge weights (the reciprocal of the distance) less than 1, with weaker connections for greater distances. To avoid numerical anomalies in special structures, the maximum edge weight is capped at 1.1 for extremely close atom pairs. Additionally, ASUAM incorporates a self-connection strategy (Liang *et al.*, 2021). These initial adjacency connections are refined to emphasize symmetry operations within the space group, treating atoms within a subgroup as a single entity while maintaining distinctions between different atoms through node definitions. Both adjacency matrices are utilized in ASUGNN. The specifics of these matrices are provided in the supporting information.

2.3. Graph (U)

One-dimensional diffraction patterns in reciprocal space are calculated for each structure, reflecting atom arrangements along various directions. The static structure factor (Cao *et al.*, 2024) encapsulates the quantized distribution of electron states. To account for structural thermal vibrations, a certain broadening is applied to each diffraction peak, resulting in a 140-dimensional global embedding of the entire reciprocal space pattern across lattice plane distances ranging from 1.2 to 8.8 Å. Through node, edge and global embeddings, ASUGNN comprehensively addresses all three aspects of crystal expression. The powder XRD calculation details are elucidated in the supporting information.

3. Architecture of ASUGNN

With the initial embedding of the node matrix \mathbf{N} , the distance adjacency matrix (DAM and ASUAM) and the global vector \mathbf{G} , ASUGNN aggregates all physical insights through a message-passing mechanism. The model employs a crystal graph convolution layer as a preliminary module to update node embeddings. These embeddings, after being processed through a fully connected layer, are fed into the ASU-codec, as illustrated in Fig. 2(a). Within the ASU-codec, interatomic distances are embedded using Gaussian basis function encoding. This approach transforms the raw distance matrix into a rich, continuous feature space that captures the intricate nuances of a crystal's topology and chemistry. Each pairwise atomic distance is represented not as a raw number but as a sum of Gaussian functions.

The ASU encoder begins by inputting node embeddings and applying self-attention computations. Here, the queries (Q) and keys (K) undergo matrix multiplication and scaling, followed by the Softmax function and another matrix multiplication with the values (V). Before Softmax is applied, convolution with the ASUAM occurs under symmetric space constraints, allowing nodes to directly access environmental information from distinct sites. Following the self-attention operation, the output is combined with the initial node embeddings via residual connections to reduce the training load of the model. This result is then processed by a

research papers

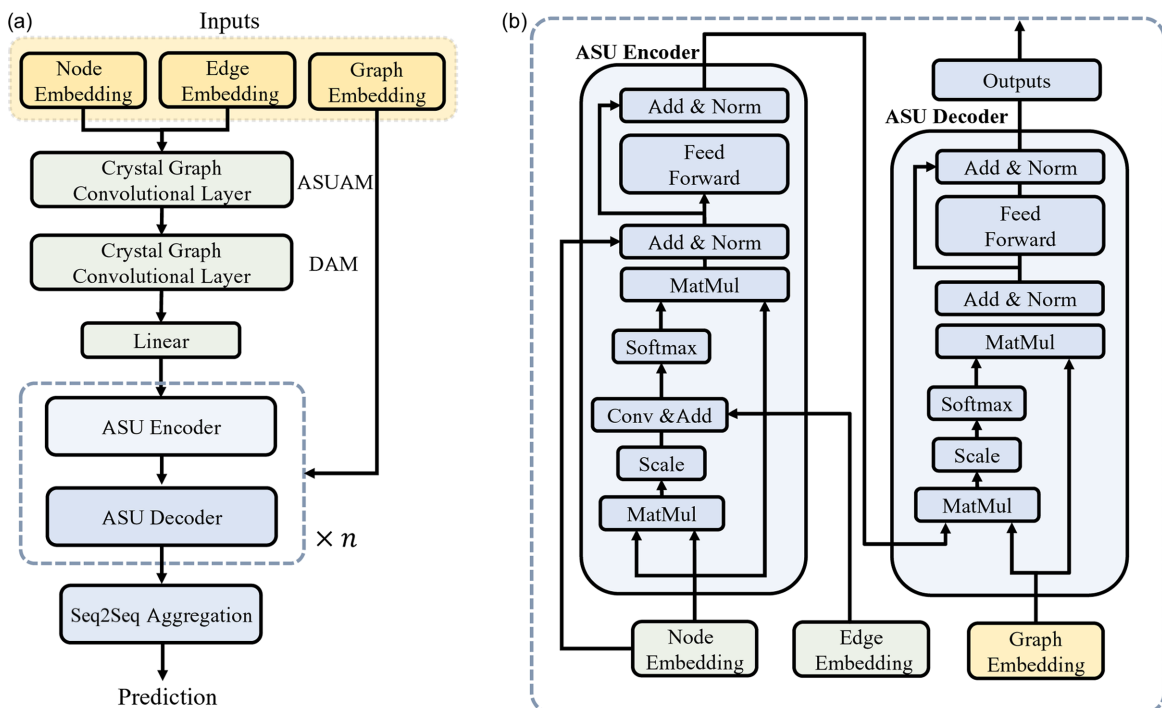


Figure 2

(a) Message-passing architecture of ASUGNN. (b) The ASU encoder takes node embeddings as input and applies self-attention computations. The ASU decoder receives the output of the encoder along with a global encoding embedding as input and performs cross-attention computations.

feed-forward module and linked again through residual connections, forming the final output of the ASU encoder. The ASU decoder block takes the encoder output and a global encoding embedding (G) as inputs to perform cross-attention computations. In this configuration, G serves as both V and K , while the encoder output acts as Q . This setup mirrors the cross-attention structure in transformers (Vaswani, *et al.* 2017), where V and K originate from the same source. Essentially, the decoder leverages the embedded real space information to interpret the reciprocal information contained in the powder XRD pattern. This process concludes with feed-forward sorting and residual connections, resulting in an updated node representation.

During cross-attention computation, information integration occurs at both the node and the graph levels within the crystal, linking the individual atomic environment information and the overall crystal environment in reciprocal space. This facilitates self-learning of the model at various hierarchical levels. After processing by $n = 2$ ASU-codec units, an aggregation operation is performed using a seq2seq pooling method based on long short-term memory (Graves & Graves, 2012), which performs a weighted summation of the final information of each node. The output is then passed through a fully connected linear layer to predict the physical properties of the crystal structure.

Heuristically, graph embeddings usually struggle to capture subtle variations in atom pairs due to their distance-based nature. However, even slight variations affect the structure factor and Ewald sphere in reciprocal space, influencing the intensity and position of each peak in the powder XRD pattern. Unlike GNN learning schemes that focus on atomic

granularity, the embedding G captures global information through powder XRD patterns. Consequently, ASUGNN not only perceives the overall crystal symmetry and spatial characteristics of atomic packing but also inherits reciprocal information.

4. Benchmark

4.1. Dataset

The MP-2024-1 dataset, sourced from the non-trajectory Materials Project database (Jain *et al.*, 2013), initially comprised 154 718 crystals with associated DFT-calculated physical properties. After a rigorous screening process, structures exhibiting broken symmetry, duplication or space group mismatches identified by comparison with those computed using *spglib* (Togo *et al.*, 2024) were excluded. This curation resulted in the MP-2024-1 dataset containing 111 120 unique crystal structures. The dataset was split in an 8:2 ratio for training and testing. For assessing sensitivity to structural changes, datasets derived from randomly generated systems of Ag and Fe-C amount to a total of 1100 structures. These structures were relaxed using the Vienna *Ab Initio Simulation Package* (VASP; Kresse & Furthmüller, 1996*a,b*; Kresse & Hafner, 1993) to achieve convergence at the electronic step, resulting in the HMdataset (home-made structures dataset).

The formation energy (E_f) of a configuration represents the energy required or released to generate that configuration. Thus, the formation process can be either endothermic or exothermic. The more negative the formation energy of a structure, the more stable the structure, indicating its thermal

Table 1

Ablation study on the order of ASUAM and DAM, and the embedding dimensions of the ASU-codec.

The results are evaluated on the basis of the MAE metric.

First AM	Second AM	MAE (eV per atom)
DAM	DAM	0.044
DAM	ASUAM	0.022
DAM	-	0.056
ASUAM	DAM	0.017
ASUAM	ASUAM	0.019
ASUAM	-	0.021

Dimensions	Trainable parameters	MAE (eV per atom)
384	1.05×10^7	0.032
512	1.86×10^7	0.017
768	4.17×10^7	0.021

stability (Seitz & TTurnbull, 1956). Figs. 3(a) and 3(b) illustrate the formation energy per atom across 111 120 crystal structures in MP-2024-1 and 1100 crystal structures in the HMdataset. The formation energy of structures in the HMdataset is higher as it contains more sub-stable structures with structural changes, posing a greater challenge for ML-based property prediction.

4.2. Ablation studies

Before the ASU-codec, the graph convolutional layers were used to activate atom pair connections and enhance crystal embeddings. Table 1 presents ablation studies that evaluate the sequence order of two matrices in the CGCNN layers, along with a case where only one adjacent matrix is applied. These studies show the impact on formation energy prediction performance within the MP test set. Results indicate that, while the DAM captures extensive distance information, concatenating it with the ASUAM based on the ASU provides superior predictive performance.

In the ASU-codec, we conducted ablation studies comparing Q , K and V embedding dimensions of 384, 512 and 768, as listed in Table 1. Balancing model efficiency and performance, we ultimately selected a node embedding

dimension of 512. The attention mechanism utilized 8 attention heads, and overfitting was mitigated through the use of a dropout mechanism (Li *et al.*, 2023).

To further investigate the merits of introducing powder XRD in the graph embedding of crystals, we eliminated the global XRD information by employing a mask matrix, ensuring that the attention scores after softmax converged to zero in the decoder, without modifying the model architecture. The results showed a significant decrease in formation energy prediction, with a mean absolute error (MAE) of $0.043 \text{ eV atom}^{-1}$, indicating the importance of incorporating the XRD sequence.

4.3. Baselines

We consider three state-of-the-art models for crystal property prediction as baselines, as each, like ASUGNN, is trained on non-trajectory data from the Materials Project database.

CGCNN: an early model by Xie *et al.* (Xie & Grossman, 2018) that applies GNNs to embed crystal structures and has become a classic baseline in the field.

MEGNet: developed by the Materials Project (Chen *et al.*, 2019) and widely used for its robust performance in crystal property prediction.

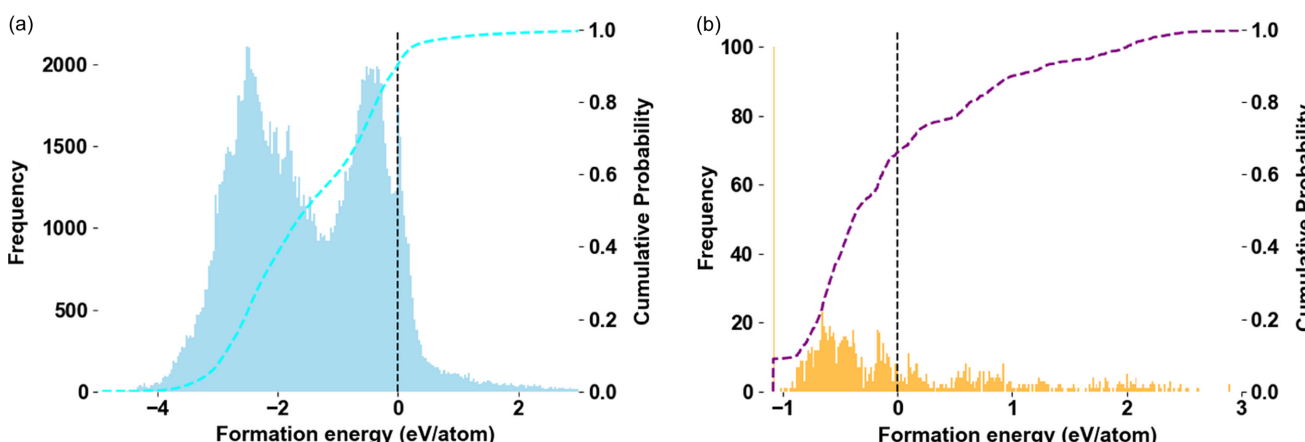
ALIGNN: a community-recognized model (Choudhary & DeCost, 2021) known for embedding bond angles into graph representations, offering enhanced structure information.

4.4. Implementation details

We use the following hyper-parameters across all experiments: batch size 128, learning rate 1.5×10^{-4} . All models are trained for 200 epochs with an early stopping patience of 10. We use the MAE and R^2 as metrics to evaluate the performance of the models. All model implementations are based on the Pytorch (Paszke *et al.*, 2019) library, trained on the GeForce RTX 4090 GPU.

5. Results

The sensitivity of the model to various elemental compositions and structural variations is evaluated through our tests.

**Figure 3**

Statistics of the datasets. Distribution of formation energy per atom of crystals in (a) MP-2024-1 and (b) HMdataset.

Evaluating the ability of a model to predict multi-component systems (*e.g.* MP-2024-1) is crucial for assessing its performance in diverse chemical environments, especially regarding the interactions and reaction kinetics of various elements. High-throughput screening scenarios often involve integrated datasets with mixed elements. Furthermore, the model must accurately predict the dynamic evolution of sub-stable structures (*e.g.* HMdataset) within multi-substance systems.

5.1. On MP-2024-1

Fig. 4 demonstrates the prediction capabilities of ASUGNN for the multi-component dataset MP-2024-1. Figs. 4(a)–4(c) illustrate the error levels in the regression predictions, and Fig. 4(d) displays the classification result. We established four crystal property tasks to comprehensively evaluate the performance of ASUGNN in understanding crystal structures: formation energy prediction, bulk modulus prediction, band-gap prediction and metal–non-metal classification tasks.

The bulk modulus under Voigt's approximation is derived from the elastic matrix. It is calculated as follows:

$$K_V = \frac{1}{9} [C_{11} + C_{22} + C_{33} + 2(C_{12} + C_{13} + C_{23})],$$

where C_{ij} represent the elastic constants of the material, derived from the elastic matrix. Here, C_{11} , C_{22} and C_{33} represent the elastic constants relating normal stress to normal strain along the principal axes, whereas C_{12} , C_{13} and C_{23} are

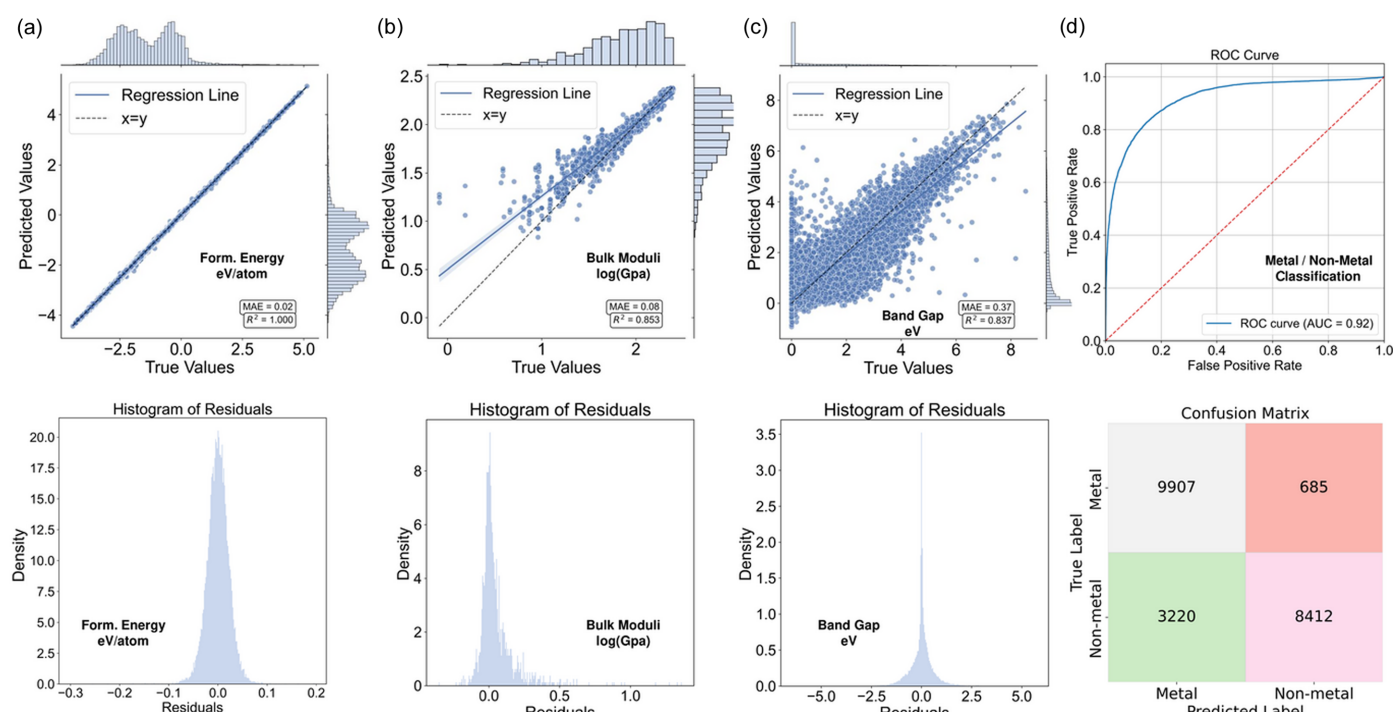


Figure 4

(a) Comparison of predicted formation energy values with DFT-calculated values, along with the distribution of prediction residuals for formation energy prediction tasks. (b) Comparison of predicted bulk moduli (in logarithmic scale) with DFT-calculated values, accompanied by the distribution of prediction residuals for bulk modulus prediction tasks. (c) Comparison of predicted band-gap values with DFT-calculated values, along with the distribution of prediction residuals for band-gap prediction tasks. (d) ROC curve and confusion matrix for metal versus non-metal classification tasks. Note: only 9479 crystal records in the MP-2024-1 dataset contain bulk modulus values.

Table 2

MAE values for three regression tasks and accuracy for one classification task on the MP-2024-1 dataset.

Model	Formation energy MAE (eV per atom)	Bulk modulus MAE [log(GPa)]	Band-gap MAE (eV)	Metal/non-metal accuracy (%)
CGCNN	0.031 ± 0.004	0.054^\dagger	0.388^\dagger	—
MEGNet	0.028 ± 0.003	0.050^\ddagger	0.330^\ddagger	78.9^\ddagger
ALIGNN	0.022 ± 0.002	1.017^\S	0.140^\S	92.0^\S
ASUGNN	0.020 ± 0.003	0.081 ± 0.006	0.370 ± 0.033	82.4 ± 3.4

† Results retrieved from Xie & Grossman (2018). ‡ Results retrieved from Chen *et al.* (2019). § Results retrieved from Choudhary & DeCost (2021). The training data used in their paper are from the JARVIS dataset, and we calculated the logarithm of the bulk modulus to align with our settings.

the coupling terms between normal stress and strain in anisotropic materials.

The band gap is defined as the energy difference between the valence band and the conduction band. A metal crystal has a zero band gap, whereas a non-metal exhibits a specific band gap. Fig. 4(a) presents the predicted values for formation energy, Fig. 4(b) those for bulk modulus and Fig. 4(c) those for band-gap predictions. ASUGNN achieved superior prediction accuracy, with errors approximately normally distributed around a mean of zero, demonstrating high robustness. For the classification task, the receiver operating characteristic (ROC) curve shows an area under the curve of 0.92, and the confusion matrix indicates a classification accuracy of 82.4% for ASUGNN.

We also benchmarked the predictive ability of ASUGNN against three baseline models on the MP-2024-1 test set, as shown in Table 2. Using fivefold cross-validation, we tested the model five times, reporting the mean and standard deviation of the prediction MAE values. The results demonstrate that ASUGNN has advantages in formation energy regression tasks and metal/non-metal classification tasks.

5.2. HMdataset

The generalization ability of a model is crucial for its practical application. To validate the adaptability and predictive accuracy of the model across different datasets, we employed a model trained on MP-2024-1 to predict the properties of Ag and Fe-C systems, specifically testing the model's zero-shot prediction capability on sub-stable dynamic evolution structures. Our tests show that, like Chen *et al.* (2019) found, most baselines were not sensitive to structural variations. Although ALIGNN outperformed the other baseline models, it remained unsatisfactory, achieving a total MAE of 0.76 eV per atom which is comparable to 0.81 eV per

atom for CGCNN and 0.78 eV per atom for MEGNet. The results indicated that all baselines trained without trajectory data had significant limitations in predicting the evolution of sub-stable structures. However, the integration of powder XRD into global graph information within ASUGNN enhances the capacity of the model to capture the discontinuous nature of graphs while retaining the benefits of sequence models. Consequently, we compared our ASUGNN with M3GNet, despite M3GNet being an interatomic potential network trained on extensive trajectory data.

As shown in Figs. 5(a) and 5(b), M3GNet demonstrated superior performance on the mixed dataset composed of Ag and Fe-C systems. Even in zero-shot testing scenarios, it achieved a total MAE of 0.47 eV per atom, showing excellent generalization capabilities (MAE = 0.428 for the Ag system and MAE = 0.523 for the Fe-C system). In contrast, ASUGNN achieved a lower total MAE of 0.35 eV per atom in zero-shot predictions (MAE = 0.452 for the Ag system and MAE = 0.238 for the Fe-C system) and a higher R^2 score. Notably, ASUGNN was trained on the public non-trajectory MP-2024-1 dataset, which contains significantly fewer structures (in the

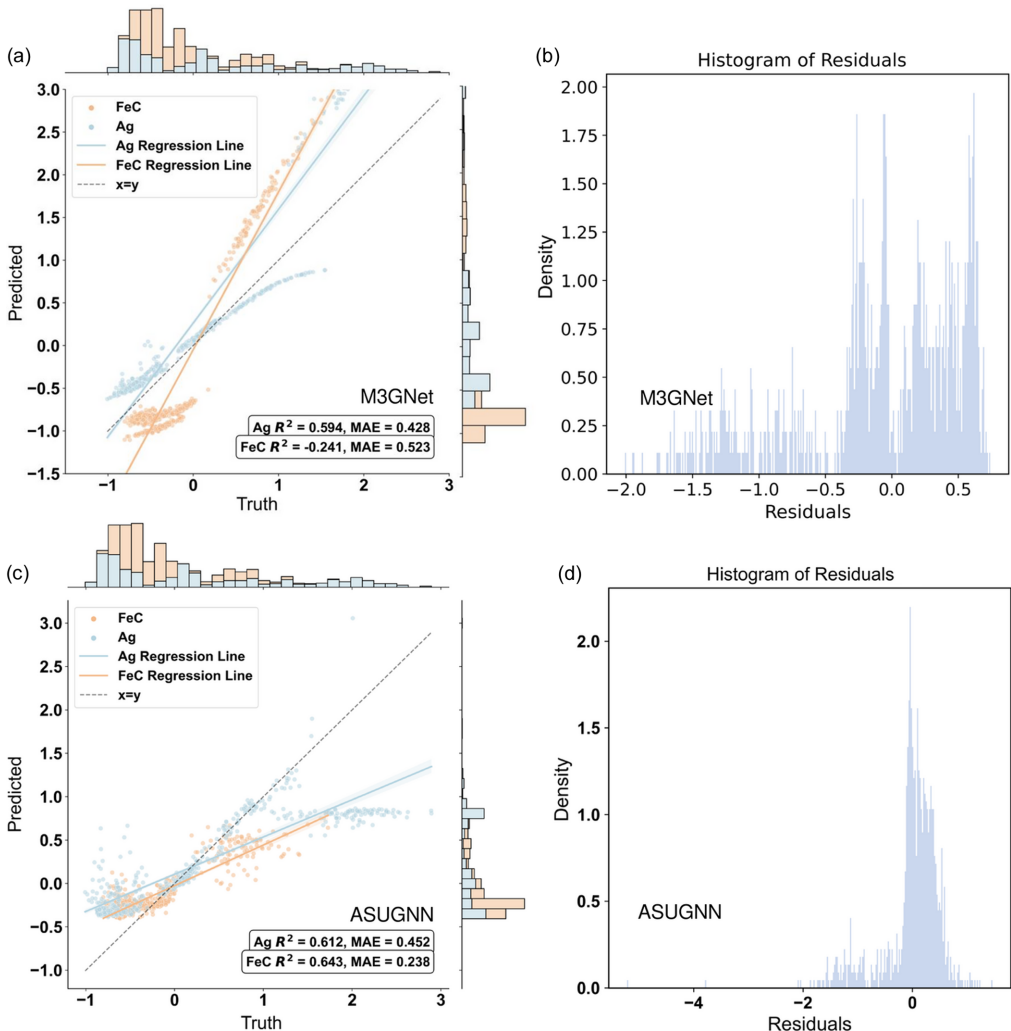


Figure 5

(a) Predicted E_f values versus DFT-calculated E_f values of M3GNet. (b) Distribution of prediction residuals of M3GNet. (c) Predicted E_f values versus DFT-calculated E_f values of ASUGNN. (d) Distribution of prediction residuals of ASUGNN.

hundred-thousands) compared with the million-level dataset used for M3GNet, yet still demonstrated a superior ability to recognize sub-stable structures, as shown in Figs 5(c) and 5(d). ASUGNN tends to predict lower values in the high-energy zone compared with M3GNet. This discrepancy arises because the ASUGNN training set consists of non-trajectory datasets that primarily include stable, low-energy structures, as shown in Fig. 3. Though M3GNet performs better in the high-energy zone, ASUGNN demonstrates greater accuracy in the low-energy zone, contributing to its overall superior performance.

Although the HMdataset contains relatively limited chemical systems and structures, which may include some randomness, the results illustrate that ASUGNN demonstrates comparable ability in zero-shot predictions to trajectory models such as M3GNet. Fig. 5(c) illustrates the high sensitivity of ASUGNN to structural changes. Additionally, examining the residual distribution plots reveals that the residuals in Fig. 5(d) are more concentrated and symmetric with a peak close to zero, suggesting smaller and more uniformly distributed prediction errors. This indicates that the model errors are more likely to be randomly distributed, without significant systematic bias. In contrast, the residual distribution of M3GNet in Fig. 5(b) is more dispersed with multiple peaks, indicating larger and unevenly distributed prediction errors. This could be due to localized overfitting or underfitting as the model processes more data.

6. Concluding remarks

In this study, we introduced an ASU-based physical graph embedding and developed ASUGNN, which demonstrates great potential in crystal property prediction tasks. Three key factors are essential in crystal graph embedding: the spatial arrangement of distinct atoms, symmetry constraints from the space group and governing electronic equations. To incorporate these factors, we created the ASU adjacency matrix to represent space group constraints and used powder XRD as a global embedding to illustrate the relationship between electronic distributions, atom types and arrangements. Consequently, ASUGNN, despite being trained on a smaller subset of the non-trajectory dataset MP-2024-1, exhibited significant sensitivity to structural changes and achieved impressively low error rates in zero-shot predictions. Our experiments with ASUGNN provide valuable insights for model architecture in computational materials science, guiding future research and development efforts aimed at designing more robust models to tackle the complexities of real-world materials discovery and design challenges.

7. Related literature

The following references are cited in the supporting information: Armstrong (1967); Caglioti *et al.* (1958); Hubbell *et al.* (1974); Miranda *et al.* (2018).

Conflict of interest

The authors declare no competing interests.

Data availability

The HMdataset examined in the paper is available at <https://huggingface.co/caobin/ASUGNN>. The Model described in the present work was implemented in Python. Source codes are available at <https://github.com/AI4Cr/ASUGNN>. The HMdataset is open-sourced on our Hugging Face repository for zero-shot testing, and we organized a Kaggle competition to fairly evaluate its capabilities. For more details, visit the competition page: <https://www.kaggle.com/competitions/asugnn>.

Funding information

Funding from Guangzhou Hong Kong University of Science and Technology (GZ-HKUST) Joint Funding Program (grant No. 2023A03J0003) is acknowledged.

References

- Armstrong, B. (1967). *J. Quant. Spectrosc. Radiat. Transfer*, **7**, 61–88.
- Bloch, J., Cavalleri, A., Galitski, V., Hafezi, M. & Rubio, A. (2022). *Nature*, **606**, 41–48.
- Bohr, N. (1913). *London Edinb. Dubl. Philos. Mag. J. Sci.* **26**, 1–25.
- Caglioti, G., Paoletti, A. & Ricci, F. (1958). *Nucl. Instrum.* **3**, 223–228.
- Cao, B., Liu, Y., Zheng, Z., Tan, R., Li, J. & Zhang, T. (2024). *arXiv*, 2406.15469.
- Chen, C. & Ong, S. P. (2022). *Nat. Comput. Sci.* **2**, 718–728.
- Chen, C., Ye, W., Zuo, Y., Zheng, C. & Ong, S. P. (2019). *Chem. Mater.* **31**, 3564–3572.
- Choudhary, K. & DeCost, B. (2021). *npj Comput. Mater.* **7**, 185.
- Goodall, R. E., Parackal, A. S., Faber, F. A., Armiento, R. & Lee, A. A. (2022). *Sci. Adv.* **8**, eabn4117.
- Graves, A. & Graves, A. (2012). *Supervised sequence labelling with recurrent neural networks*, pp. 37–45. Springer.
- Hubbell, J. H., McMaster, W. H., Del Grande, N. K. & Mallett, J. H. (1974). *X-ray cross sections and attenuation coefficients*, in *International tables for X-ray crystallography*, Vol. IV, edited by J. A. Ibers & W. C. Hamilton, ch. 2.1, pp. 47–70. Kynoch Press.
- Jain, A., Ong, S. P., Hautier, G., Chen, W., Richards, W. D., Dacek, S., Cholia, S., Gunter, D., Skinner, D., Ceder, G. & Persson, K. A. (2013). *APL Mater.* **1**, 011002.
- Jiao, R., Huang, W., Liu, Y., Zhao, D. & Liu, Y. (2024). *The 12th international conference on learning representations (ICLR2024)*, 7–11 May 2024, Vienna, Austria.
- Kaba, O. & Ravanbakhsh, S. (2022). *Adv. Neural Inf. Process. Syst.* **35**, 4150–4164.
- Kresse, G. & Furthmüller, J. (1996a). *Comput. Mater. Sci.* **6**, 15–50.
- Kresse, G. & Furthmüller, J. (1996b). *Phys. Rev. B*, **54**, 11169–11186.
- Kresse, G. & Hafner, J. (1993). *Phys. Rev. B*, **47**, 558–561.
- Li, B., Hu, Y., Nie, X., Han, C., Jiang, X., Guo, T. & Liu, L. (2023). *Proceedings of the IEEE/CVF conference on computer vision and pattern recognition (CVPR2023)*, 17–24 June 2023, Vancouver, BC, Canada, pp. 22700–22709. IEEE.
- Liang, Z., Du, J., Shao, Y. & Ji, H. (2021). *Neurocomputing*, **431**, 128–136.
- Louis, S.-Y., Zhao, Y., Nasiri, A., Wang, X., Song, Y., Liu, F. & Hu, J. (2020). *Phys. Chem. Chem. Phys.* **22**, 18141–18148.
- Martin, R. M. (2020). *Electronic structure: basic theory and practical methods*. Cambridge University Press.

- Merchant, A., Batzner, S., Schoenholz, S. S., Aykol, M., Cheon, G. & Cubuk, E. D. (2023). *Nature*, **624**, 80–85.
- Miranda, M. A. R. & Sasaki, J. M. (2018). *Acta Cryst. A* **74**, 54–65.
- Paszke, A., Gross, S., Massa, F., Lerer, A., Bradbury, J., Chanan, G., Killeen, T., Lin, Z., Gimelshein, N., Antiga, L., et al. (2019). *Proceedings of the 33rd international conference on neural information processing systems (NIPS'19)* 8–14 December 2019, Vancouver, Canada, pp. 8024–8035. Curran Associates Inc.
- Seitz, F. & Turnbull, D. (1956). Editors. *Solid state physics*, Vol. 3, pp. 225–306. Academic Press.
- Togo, A., Shinohara, K. & Tanaka, I. (2024). *Spplib: a software library for crystal symmetry search*, <https://github.com/spplib/spplib>.
- Vaswani, A., Shazeer, N., Parmar, N., Uszkoreit, J., Jones, L., Gomez, A. N., Kaiser, Ł. & Polosukhin, I. (2017). *Proceedings of the 31st international conference on neural information processing systems (NIPS'17)*, 4–9 December 2017, Long Beach, CA, USA, pp. 6000–6010. Curran Associates Inc.
- Xie, T. & Grossman, J. C. (2018). *Phys. Rev. Lett.* **120**, 145301.
- Yan, K., Liu, Y., Lin, Y. & Ji, S. (2022). *Proceedings of the 36th international conference on neural information processing systems (NIPS'22)*, 28 November–9 December 2022, New Orleans, LA, USA, pp. 15066–15080. Curran Associates Inc.
- Zhu, R., Nong, W., Yamazaki, S. & Hippalgaonkar, K. (2023). *arXiv*, 2311.17916.